Effects of Walnut Shell Powder Content on the Molding Performance of Digital Light Processing 3D Printed Parts

Yueqiang Yu,[a,b] Shaorui Shen,[a] Sheng Gao,[a,b,*] Ting Jiang,[a,b] Tao Qin,[a] Junyuan Chen,[a] Chenxiang Yuan,[a] and Junkai Zhang [a]

Additive Manufacturing (AM) is a digital manufacturing method that creates structures by adding material layer by layer. This approach offers simplicity, speed, and efficiency. Additive manufacturing methods can process wood-plastic composites, but they are often limited by poor surface quality, low interfacial bonding, and the requirement for complex post-processing. In this study, walnut shell and photosensitive resin were used to fabricate wood-plastic composite specimens with varying walnut shell powder contents using DLP technology. The properties analyzed included dimensional shrinkage, mechanical strength, double bond conversion rate, and microstructure. The results indicated that as the walnut shell content increased, the dimensional shrinkage of the formed parts initially decreased and then increased, reaching the minimum value of 0.631% at 12% walnut shell powder content. SEM imaging revealed that resin infiltrates the particle pores, forming a network structure that enhances mechanical performance. Tensile and flexural strengths also reached their peak values at 8% content, measuring 17.7 and 45.4 MPa, respectively, while impact strength decreased with increasing walnut shell content.

DOI: 10.15376/biores.20.3.5348-5360

Keywords: 3D printing; Biomass composite; Walnut shell powder; Molding quality; DLP technology

*Contact information: a: College of Mechanical Science and Engineering, Northeast Petroleum University, Daqing, 163318, China; b: Key Laboratory of Petroleum Mechanical Engineering of Heilongjiang Province, Daqing, 163318, China; *Corresponding author: gaosheng_7012@163.com*

INTRODUCTION

The traditional molding process for lignocellulosic composites typically only allows for the manufacture of simple structural wood-plastic parts. In contrast, additive manufacturing offers advantages such as simple processes, short cycles, high material utilization, and the ability to form complex structures. Additive manufacturing technology directly forms materials layer by layer, making it easy to produce parts of lignocellulosic composites with intricate internal structures and curved surfaces, thereby enabling more complex designs and enhancing the functionality and performance of the parts.

Additive manufacturing technology shows a diversified trend in the molding of lignocellulosic composites, with key techniques including Fused Deposition Modeling (FDM), Laminated Object Manufacturing (LOM), and Selective Laser Sintering (SLS). Existing studies have utilized various modified composite materials with different reinforcement phases. For example, FDM composites were prepared by using modified pine wood flour (PWF), a small amount of nano-silica (nano-SiO_2), and poly(lactic acid)

(PLA) (Li *et al*. 2019); COS/PLA composites were developed by using modified camellia seed shells (COS) and PLA (Xiao *et al*. 2023). The CNF/PLA composite was prepared by melt extrusion method of PLA and cellulose nanofibers (CNF) (Wang *et al*. 2020). Boxwood/thermoplastic polyurethane powder (B/TPU) was prepared from poplar waste for laser sintering (Zhang *et al*. 2021). Composite material (WSPC) was prepared from walnut shell and copolyester hot melt adhesive (Co-PES) for selective laser sintering (Yu *et al*. 2017). However, in the FDM and SLS molding of lignocellulosic materials, due to the characteristics of the technology itself, issues such as uneven distribution and poor interfacial bonding are faced, resulting in poor part quality and necessitating additional complex post-processing (Wang *et al*. 2018; Wang *et al*. 2019). In contrast, Digital Light Processing (DLP) technology offers advantages such as smooth surfaces and fast forming speeds by curing layer by layer through photopolymerization. It is widely applied in automotive, aerospace, medical, jewelry, and other fields. DLP technology uses liquid photopolymer resins as printing materials, and researchers are developing composite photopolymer resins with different fillers to enhance their comprehensive performance. Common fillers include polymer materials, metal particles, fibers, and inorganic nanoparticles.

Lignocellulosic composites are a new type of environmentally friendly, biodegradable, and low-cost material made from agricultural and forestry waste combined with a polymer matrix (Deng *et al*. 2018). As the development of natural resources is limited, utilizing agricultural and forestry waste, such as walnut shells, to develop new composite materials has become a feasible solution. Walnut shells are biodegradable, have high hardness, and low density, making them suitable as fillers to improve the performance of composites and reduce dependence on traditional wood.

This paper uses photopolymer resin as the matrix and waste walnut shell powder as the reinforcement phase to prepare composites suitable for DLP 3D printing and analyzes the impact of different powder contents on the performance of the molded parts. By studying the micro-morphological changes in the fracture surfaces of tensile specimens with varying walnut shell powder contents, the relationship between the performance of the specimens and the powder content is established, and the optimal content ratio is determined, providing a reference for the application of walnut shell powder in DLP.

EXPERIMENTAL

Materials

Experimental materials

The walnut shell powder (approximately spherical particles, particle size range of 74 to 90 μm, apparent density of 0.56 g/cm³) was obtained from a water treatment materials company. Industrial alcohol (a clear liquid with an alcohol content greater than 99% and a density of 0.791 g/cm³) was supplied by Harbin Datong Chemical Co., Ltd. (Harbin, China). The standard rigid photosensitive resin (main components include polyurethane acrylate (PUA), trimethylolpropane triacrylate (TMPTA), modified acrylate, additives, and photoinitiators, with a viscosity of 100 to 250 MPa·s at 25 °C) was provided by Shenzhen Yidimu Intelligent Technology Co., Ltd (Shen Zhen, China).

Composite material preparation

The composite material was composed of walnut shell powder and a transparent photosensitive resin. Walnut shell waste was processed through crushing, screening, washing, and filtering to produce porous, yellow-brown particles. The transparent photosensitive resin facilitated observation of the mixture's state. In this study, dried walnut shell powder was mixed with the resin at varying mass percentages. To prevent powder agglomeration due to high surface energy and static forces, a combination of magnetic stirring and ultrasonic dispersion was used: the mixture was magnetically stirred for 0.5 h at a temperature below 30 °C, then further dispersed in an ultrasonic cleaner. The cavitation effect of ultrasonication breaks up agglomerates, ensuring uniform powder distribution. Ultrasonic dispersion also raises the temperature slightly, reducing resin viscosity and promoting dispersion. Finally, the mixture was left to stand for degassing and was stored in the dark. The proportions of each component are listed in Table 1.

Table 1. The Factors and Levels of Digital Light Processing Test

Test number	I	II	III	IV	V	VI	VII	VIII	IX	X	XI
Percentage by weight of powder (%)	0	2	4	6	8	10	12	14	16	18	20
Percentage by weight of resin (%)	100	98	96	94	92	90	88	86	84	82	80

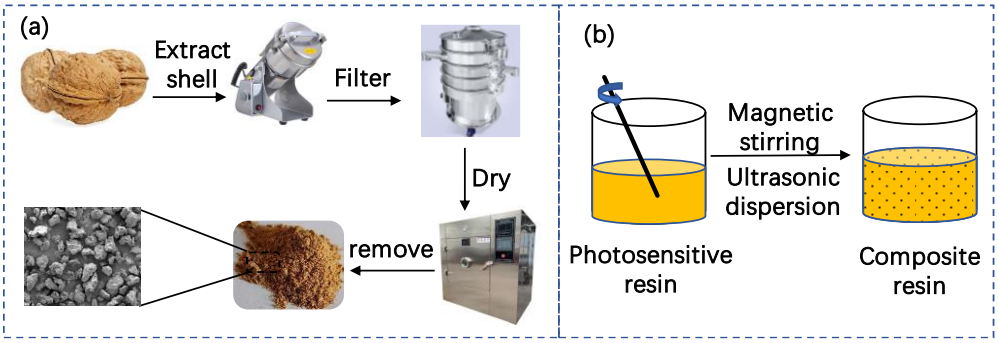

Fig. 1. Preparation process of walnut shell/photosensitive resin composite: (a) preparation process of walnut shell powder; (b) composite material mixing process

Methods

DLP3D printing molding experiment

The digital light processing (DLP) process for composite parts with different ingredient ratios was conducted using a DLP printing device developed by Jiang's research group (Jiang *et al*. 2022). The equipment and forming process are illustrated in Fig. 2. The main process parameters were as follows: light intensity of 50 mW/cm², layer thickness of 150 µm, single-layer exposure time of 4.5 seconds, base layer exposure time of 38 seconds, and processing temperature of 25 °C.

Figure 2 illustrates the principle of DLP 3D printing. The forming process involves first designing a 3D solid model using 3D software, which is then sliced by a discretization program to create a pattern for light exposure. The generated data precisely controls the movement of the light source and the lifting platform. Resin is then added to the resin tank, where the light source irradiates it, causing photopolymerization within the thin region of the resin tank, forming a thin layer of the part. The printing platform then moves up by one layer, allowing the light source to continue exposure and process the next layer. This cycle repeats, layer by layer, until the complete 3D part is formed.

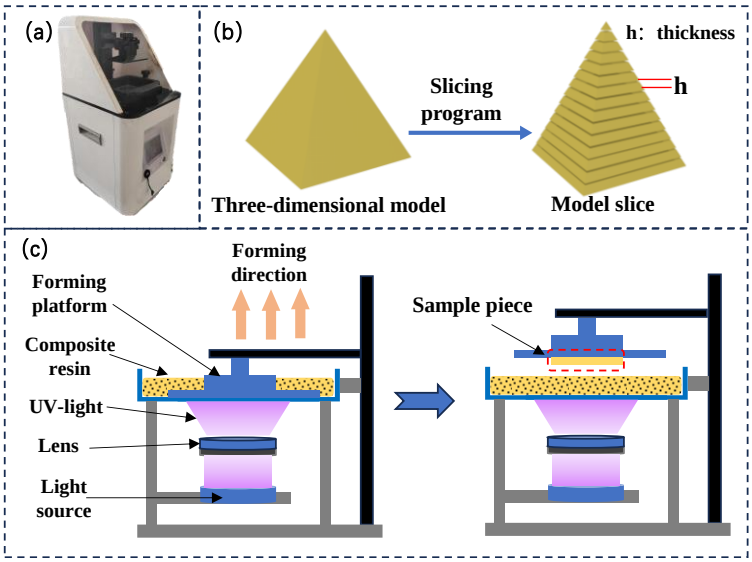

Fig. 2. Equipment diagram and forming process (a) DLP printing equipment; (b) Model slicing process; (c) DLP forming process

Viscosity

The dynamic viscosity of resin systems containing varying proportions of walnut shell powder was measured using rotational rheometry with a DV-2 Pro rotary viscometer (Brookfield Engineering Laboratories, Inc., USA). A sample volume of 50 mL was tested at a temperature of 25°C for each measurement. Three parallel tests were conducted for each experimental group, and the arithmetic mean of the results was calculated to characterize the rheological properties of the systems.

Double bond conversion rate

The Nicolet iS20 Fourier-transform infrared (FTIR) spectrometer (Thermo Fisher Scientific Ltd, USA), was used to conduct absorbance tests on molded specimens and liquid photosensitive resins with varying walnut shell powder content. The tests were performed using the Attenuated Total Reflectance (ATR) mode, and the baseline method was calculated according to Willard *et al*. (1988). The C=C stretching vibration peak at 1638 cm^{-1} was selected as the target peak, with the NH peak at 1537 cm^{-1} serving as the internal standard for calculating the extent of conversion (Sideridou *et al*. 2002; Papakonstantinou *et al*. 2013). Due to multiple factors affecting peak shape, this study used peak height for calculations. Data analysis was conducted using OMNIC software, with automatic baseline correction and peak height measurement using the two-point baseline method. The final double bond conversion rate was calculated by Eq. 1 (Hong *et al*. 2017),

$$DC = (1 - \frac{HB_1/HB_2}{HA_1/HA_2}) \times 100\% \quad (1)$$

where *DC* represents the Double Bond Conversion percentage (%), HB_1 denotes the peak height of the target after curing, and HB_2 indicates the peak height of the internal standard after curing. HA_1 represents the peak height of the target before curing, HA_2 is the peak height of the internal standard before curing.

Mechanical properties

The mechanical properties of composite parts with different component ratios were tested using the CMT 5504 tensile testing machine from TMS System Ltd. and the TCJ-4 impact testing machine from Jilin Taihe Co., Ltd. (Changchun, China). The tensile strength was measured according to ISO 527-2 standards. The crosshead speed was set at 5 mm/min with a gauge length of 50 mm. The dimensions of the tensile specimen, shown in Fig. 3(a), were 80 mm × 5 mm × 4 mm. The three-point bending strength was measured according to ISO 178 standards. The crosshead speed was also set at 5 mm/min, with a span length of 64 mm. The dimensions of the bending specimen, illustrated in Fig. 3(b), were 80 mm × 10 mm × 4 mm. The U-notch impact strength was measured according to ISO 179-2 standards. The pendulum impact energy was set to 4 J, with a span length of 60 mm. The dimensions of the impact specimen, shown in Fig. 3(c), were 75 mm × 10 mm × 3 mm.

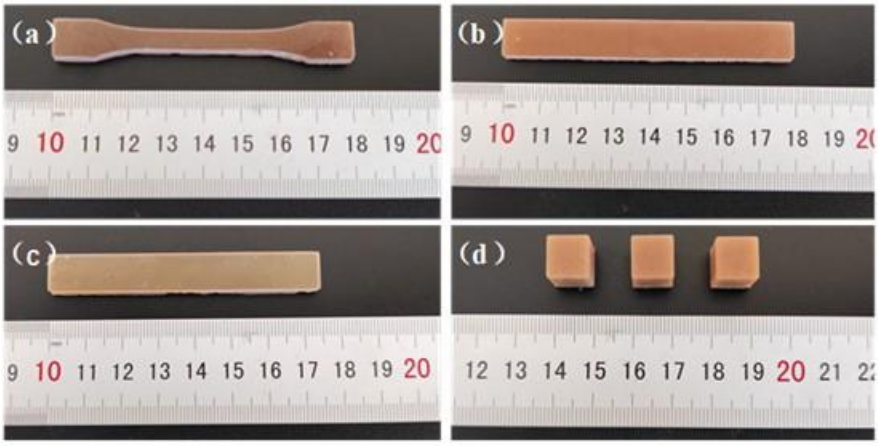

Fig. 3. Test sample model diagram; (a) tensile specimens; (b) Bending specimens; (c) Impact test pieces; (d) Dimensional shrinkage test specimen

Dimensional shrinkage

As shown in Fig. 3(d), the length (X), width (Y), and height (Z) of the sample were measured five times using a digital caliper, and the average values were taken. The theoretical dimensions of the sample are 1 cm × 1 cm × 1 cm. The dimensional shrinkage (%) was calculated using Eq. 2 (Xu *et al*. 2021),

$$L = \left(\frac{|X-X_0|}{3X_0} + \frac{|Y-Y_0|}{3Y_0} + \frac{|Z-Z_0|}{3Z_0}\right) \times 100\% \quad (2)$$

where L denotes the percent shrinkage, X_0, Y_0, and Z_0 represent the theoretical dimensions of the sample, and X, Y, and Z are the actual dimensions of the sample.

Scanning electronic microscopy (SEM)

Since the samples were initially non-conductive, they were gold-coated for 45 seconds using a Quorum SC7620 sputter coater at a current of 10 mA prior to testing. The cross-sections of composite powders and formed components with different composition ratios were scanned using a ZEISS GeminiSEM 300 (Germany) scanning electron microscope. The instrument employs a Schottky field emission electron gun with an acceleration voltage of 3 kV. SEM images were obtained to characterize the powder particle morphology and internal microstructure of composite material components with varying composition ratios.

Density

Using the DMA 4200M density analyzer (Anton Paar GmbH, Austria) based on Archimedes' principle—gas expansion displacement method, density measurements were conducted on composite material molded parts containing varying proportions of walnut shell powder. Cubic specimens with dimensions of 10 mm × 10 mm × 10 mm were prepared. Three parallel measurements were performed for each sample group, and the arithmetic mean of the results was adopted as the density characterization parameter.

RESULTS AND DISCUSSION

Double Bond Conversion Rate

The infrared spectra of samples with different walnut shell powder contents before and after forming are shown in Fig. 4.

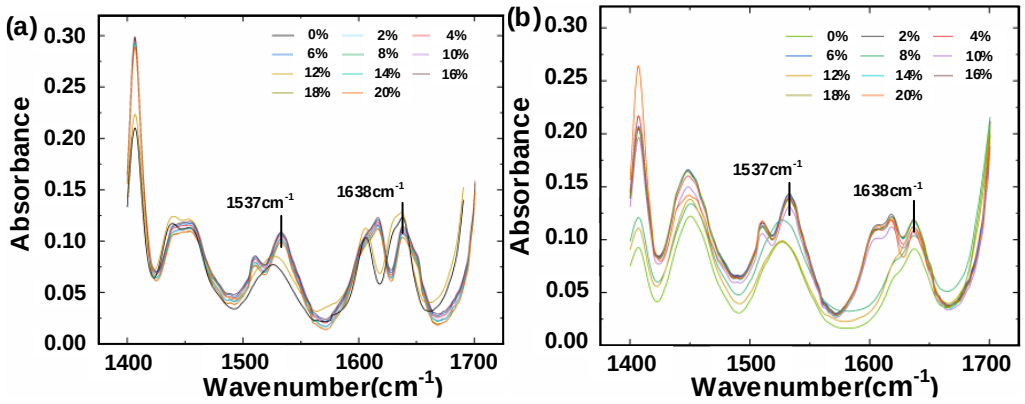

Fig. 4. Infrared spectra of walnut shell/photosensitive resin molded parts with varying ratios; (a) Infrared spectrum before forming; (b) Infrared spectrum after forming

The double bond conversion data for formed components with varying powder contents are summarized in Table 2. The extents of conversion demonstrated a significant decreasing trend with increasing walnut shell powder content, declining from 53.5% at 0% powder content to 23.6% at 20% powder content. This reduction primarily stems from UV light scattering by walnut shell particles during photopolymerization, which attenuated light penetration depth into the resin matrix and consequently diminished both irradiance intensity and conversion efficiency (Niu *et al*. 2020).

Table 2. Double Bond Conversion of Molded Parts with Different Powder Content of Walnut Shell

Powder Content	Peak	Corrected Height	Baseline	DC
Uncured Resin	1537	0.0514	1492.634,1569.290	/
	1638	0.0952	1571.219,1655.589	
0%	1537	0.0748	1489.741,1581.825	53.5%
	1638	0.0644	1587.128,1664.749	
2%	1537	0.0859	1488.777,1572.665	48.2%
	1638	0.0824	1574.111,1665.231	
4%	1537	0.0799	1487.813,1568.326	42.3%

Powder Content	Peak	Corrected Height	Baseline	DC
	1638	0.0855	1571.701,1663.785	
6%	1537	0.0779	1489.259,1568.808	40.4%
	1638	0.0861	1572.665,1664.749	
8%	1537	0.0802	1490.705,1580.379	39.6%
	1638	0.0897	1584.236,1665.231	
10%	1537	0.0768	1491.187,1569.772	38.8%
	1638	0.0871	1571.701,1664.267	
12%	1537	0.0717	1491.669,1577.486	37.0%
	1638	0.0802	1579.896,1667.642	
14%	1537	0.0734	1488.295,1569.772	29.9%
	1638	0.0953	1573.629,1665.714	
16%	1537	0.0577	1492.634,1572.183	24.1%
	1638	0.0811	1573.629,1665.231	
18%	1537	0.0702	1490.223,1566.880	24.0%
	1638	0.0989	1572.665,1668.124	
20%	1537	0.0702	1488.295,1570.737	23.6%
	1638	0.0993	1573.629,1665.231	

Viscosity

As shown in Fig. 5, the viscosity of the walnut shell/photosensitive resin composite system exhibited a significant upward trend with increasing walnut shell powder content, rising from 255 cP at 0% powder content to 510 cP at 20% powder content. Excessive viscosity impeded resin layer recoating, increasing the likelihood of air bubble entrapment and resulting in the formation of internal pores after curing. Additionally, heightened adhesion forces amplified demolding effects during the forming process, inducing defects such as warpage deformation, which ultimately degraded the structural integrity of the molded parts. Therefore, precise control of walnut shell powder content in the resin system is essential to mitigate these processing challenges and ensure optimal performance of the final product.

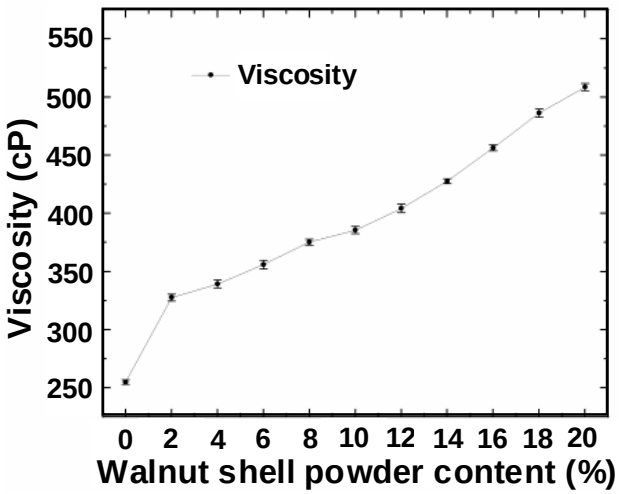

Fig. 5. Viscosity profile of walnut shell/photosensitive resin molded parts with varying ratios

DLP 3D Printing Experiment

Figure 6 shows that as the walnut shell powder content increased, part deformation decreased. When the walnut shell powder content exceeded 2%, warping was reduced

because the walnut shell powder does not participate in the molding reaction or deform, so increasing its content can reduce strain in the molded part. However, at a powder content of 16%, Fig. 6(c) showed significant deformation of the molded part. Higher powder content reduces dispersion uniformity and the resin's light transmittance, affecting the curing depth and leading to uneven UV absorption, which creates internal stress and deformation. Additionally, hollows formed by powder agglomeration further exacerbate deformation. Therefore, the walnut shell powder content should not be excessively high.

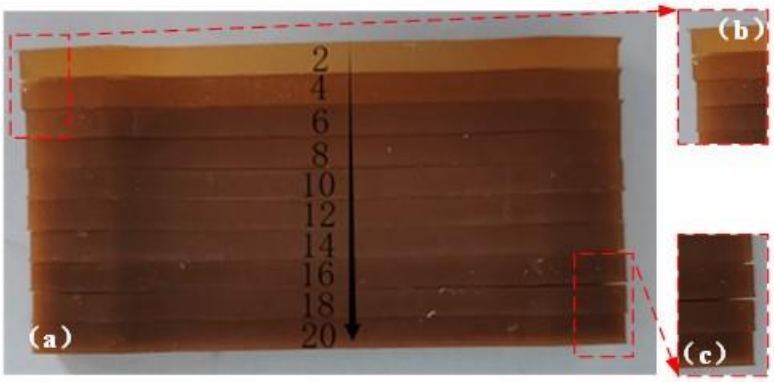

Fig. 6. (a) Tensile parts with different component ratios; (b) defects on the left side; (c) defects on the right side

Mechanical Properties

Figure 7 shows the variation in mechanical properties of molded parts with different walnut shell/resin ratios. As the walnut shell powder content increased, the impact strength of the molded parts decreased, while the tensile and bending strength initially increased and then decreased. When the powder content was below 8%, the tensile and bending strength improved. This is because, after resin curing, a honeycomb-like structure formed on the surface of the powder particles, enhancing the interfacial bonding strength between the walnut shell powder particles and the resin, thereby improving the mechanical properties (Li *et al*. 2022). Additionally, the powder particles inhibited the propagation of internal cracks in the resin during fracture, further enhancing resistance to external forces. When the powder content reached 8%, the tensile and bending strengths reached their maximum values of 17.7 and 45.4 MPa, respectively. When the powder content exceeded 8%, the mechanical properties decreased due to agglomeration that forms cavities, reducing the degree of curing. Figure 7(c) shows that the impact strength declined rapidly before the powder content reached 8% and stabilized. This is because the nearly spherical powder particles do not enhance the part's resistance to short-term external impacts.

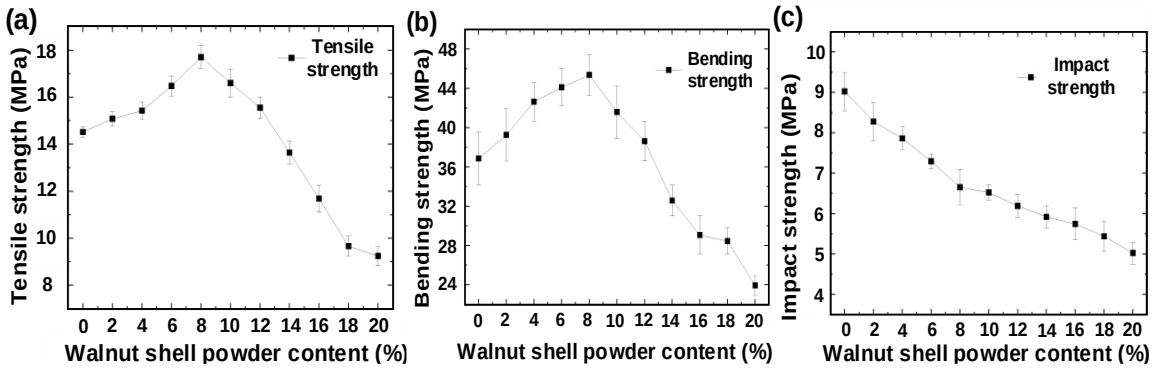

Fig. 7. Mechanical properties of walnut shell/photosensitive resin molded parts with varying ratios: (a) tensile strength; (b) bending strength; (c) impact strength

Dimensional Shrinkage Rate

During the photocuring process, the monomers, oligomers, and photoinitiators in the photosensitive resin absorb ultraviolet light, transitioning from a liquid to a solid state. This causes curing shrinkage in the molded part, making its actual dimensions smaller than the theoretical ones. Figure 8 shows that when the walnut shell powder content was below 12%, the shrinkage rate of the molded part gradually decreased, and overall accuracy improved. This is because the walnut shell powder particles do not undergo chemical reactions or deformation during curing, reducing changes in molecular distances within the resin due to changes in chemical bonds. At a powder content of 12%, the shrinkage rate reached a minimum of 0.631%. When the powder content exceeded 12%, the powder was prone to agglomeration, forming hollows and reducing the resin's light transmittance. This prevents UV light from being uniformly distributed, leading to over-curing or cavity formation, which decreases molding accuracy.

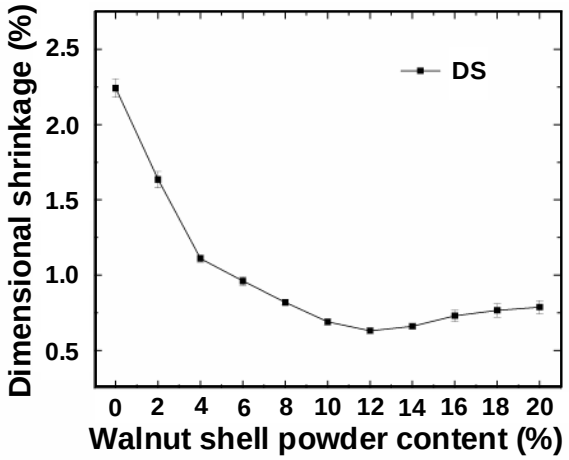

Fig. 8. Dimensional shrinkage of walnut shell/photosensitive resin molded parts with varying ratios

Scanning Electronic Microscopy

The SEM observation of the tensile fracture surfaces reveals that the fracture surfaces in Fig. 9(a-c) were relatively smooth, with no noticeable fibrillation or deformation, indicating brittle fracture characteristics. In Fig. 9(a), the molded specimen with 8% powder content shows uniformly distributed walnut shell particles, tight

interfacial bonding, and no agglomeration. In Fig. 9(b), at 12% powder content, the uniformity of particle distribution decreased, with agglomeration and hollows forming. In Fig. 9(c), the powder content of 18% showed reduced uniformity, with significant agglomeration.

Figure 9(d) demonstrates that the porous surfaces of walnut shell particles were infiltrated by liquid photosensitive resin, which then cured to form a honeycomb structure. This structure enhances interfacial bonding strength and improves mechanical properties. Fig. 9(e) shows that as walnut shell powder content increases, material transparency decreases, leading to uneven UV absorption by the photosensitive resin. This results in tighter bonding on the side facing the UV light, causing over-curing, while the side opposite the light source may have cavities due to insufficient UV absorption.

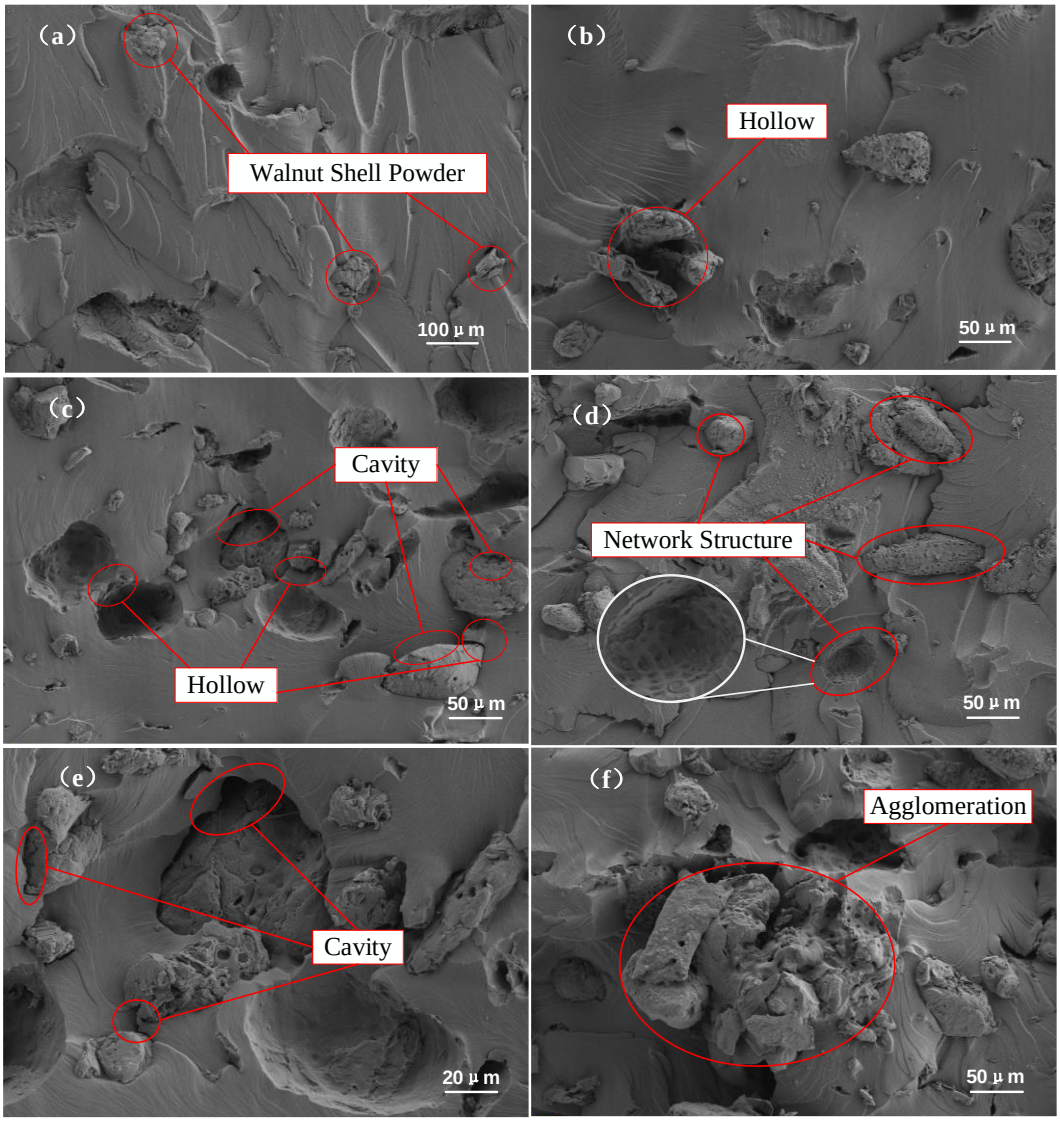

Fig. 9. Cross section scanning electron microscopy (SEM) images of walnut shell/photosensitive resin forming parts with different composition ratios: (a) 8% walnut shell powder content, magnified 200 times; (b) 12% walnut shell powder content, magnified 400 times; (c) 18% walnut shell powder content, magnified 400 times; (d) 12% walnut shell powder content, magnified 600 times; (e) 18% walnut shell powder content, magnified 1,000 times; (f) 18% walnut shell powder content, magnified 400 times

Density

The density variation of walnut shell/photosensitive resin molded parts with different ratios is shown in Fig. 10. As illustrated, the density of the molded parts decreased consistently with the increase in walnut shell powder content, with the rate of decrease gradually accelerating. This trend occurred because the density of walnut shell powder was lower than that of the photosensitive resin, and its addition reduced the overall density of the molded part. Additionally, as the powder content increased, distribution uniformity decreased, leading to an increase in hollows and cavities during the molding process, which further accelerated the reduction in density.

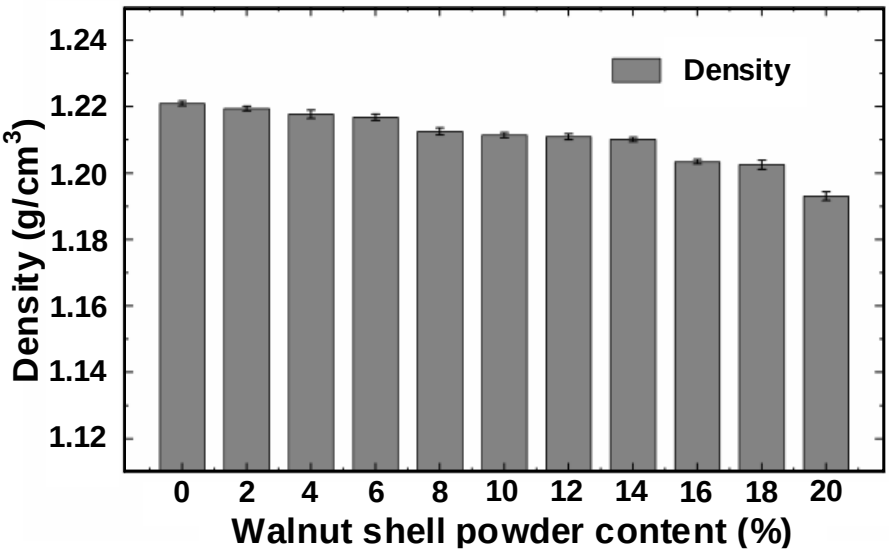

Fig. 10. Density bar chart of walnut shell/photosensitive resin molded parts with varying ratios

CONCLUSIONS

1. The cured dimensions were larger than the theoretical ones. Shrinkage minimized (0.631%) at a walnut shell content of 12%, while density decreased with higher walnut shell content.
2. The extent of double bond conversion demonstrated a sharp decrease with increasing walnut shell powder content, plummeting from 53.5% at 0% powder content to 23.6% when the powder concentration reached 20%.
3. Brittle fracturing revealed surface-proximate cross-sectional structures of the composite. Imaging showed a developed honeycomb structure near the surface, enhancing resin-particle binding tightness. However, increased walnut content promoted agglomeration, forming strength-reducing cavities and hollows.
4. Impact strength decreased as powder content rose, while tensile and flexural strengths peaked at 8% walnut shell content (17.7 and 45.4 MPa).

ACKNOWLEDGMENTS

This work was supported by the Guided Innovation Fund project of Northeast Petroleum University(2022YDL-06）, National Cultivation Fund Project of Northeast Petroleum University(2024GPL-10), the Joint Scientific and Technological Innovation Project of Hainan Province(2021CXLH0001), Key R&D Program of Heilongjiang Province, China (JD2023SJ23), General Research Project of Higher Education Reform in Heilongjiang Province (SJGYY2024186), the Scientific Research Start-up Fund Project of Northeast Petroleum University (2021KQ09 and 2019KQ67).

REFERENCES CITED

Deng, Y., Cui, R., Wang, Z., and Zhuo, A. (2018). "Research progress of polymer/biomass composites," *China Plastics* (07), 10-20. DOI: 10.19491/j.issn.1001-9278.2018.07.002

Hong, L., Wang, Y., Wang, L., Zhang, H., Na, H., and Zhang, Z. (2017). "Synthesis and characterization of a novel resin monomer with low viscosity," *Journal of Dentistry* 59, 11-17. DOI: 10.1016/j.jdent.2017.01.006

Jiang, T., Yan, B., Jiang, M., Xu, B., Xu, Y., Yu, Y., Ma, T., and Wang, H. (2022). "Enhanced adhesion—Efficient demolding integration DLP 3D printing device," *Applied Sciences* 12(15), article 7373. DOI: 10.3390/app12157373

Li, Q., Li, K., Cai, Q., Long, H., Zhao, Z., Zhou, W., and Dong, X. (2019). "Properties of PLA/PWF/nano-SiO2 wood-plastic composites for 3D printing," *Plastics Science and Technology* (01), 85-89. DOI: 10.15925/j.cnki.issn1005-3360.2019.01.013

Li, S. (2022). *Study on the Preparation of Multifunctional Silica-based Fillers and their Effect on the Properties of Dental Resin Composites*, Master's Thesis, Donghua University, Shanghai, China. DOI:10.27012/d.cnki.gdhuu.2022.000824

Niu, J., Li, D., Liu, D., Zhao, W., and Zhou Y. (2020). "Effect of SiO_2 content on properties of diphenyl composite resin," *Journal of Molecular Science* (04), 306-312. DOI: 10.13563/j.cnki.jmolsci.2020.04.008.

Papakonstantinou, A. E., Eliades, T., Cellesi, F., Watts, D. C., and Silikas, N. (2013). "Evaluation of UDMA's potential as a substitute for Bis-GMA in orthodontic adhesives," *Dental Materials* 29(8), 898-905. DOI: 10.1016/j.dental.2013.05.007

Sideridou, I., Tserki, V., and Papanastasiou, G. (2002). "Effect of chemical structure on degree of conversion in light-cured dimethacrylate-based dental resins," *Biomaterials* 23(8), 1819-1829. DOI: 10.1016/S0142-9612(01)00308-8

Wang, Q., Ji, C., Sun, L., Sun, J., and Liu, J. (2020). "Cellulose nanofibrils filled poly (lactic acid) biocomposite filament for FDM 3D printing," *Molecules* 25(10), article 2319. DOI: 10.3390/molecules25102319

Wang, Q., Sun, J., Yao, Q., Ji, C., Liu, J., and Zhu, Q. (2018). "3D printing with cellulose materials," *Cellulose* 25, 4275-4301. DOI: 10.1007/s10570-018-1888-y

Wang, S., Cao, Y., Li, X., Ma, H., Zhang, G., and Cai, T. (2019). "Research progress in preparation of wood-plastic composites used in 3D printing," *Forestry and Environmental Science* (04), 118-122.

Willard, H. H., Merritt Jr, L. L., Dean, J. A., and Settle Jr, F. A. (1988). *Instrumental Methods of Analysis*, Wadsworth Publishing Company, San Franscisco.

Xiao, J., Li, Z., Cai, Y., Hong, C., Wu, S., Guan, L., and Dong, X. (2023). "Properties of

modified *Camellia oleifera* shell powder reinforced polylactic acid 3D printing materials," *Plastics Science and Technology* (03), 18-22. DOI: 10.15925/j.cnki.issn1005-3360.2023.03.004

Xu, J., Chen, M., Zhao, Z., Li, L., Wang, S., Huang, Y., Zhao, P., Gong, C., Lu, L., and Cheng, X. (2021). "Printability and efflorescence control of admixtures modified 3D printed white Portland cement-based materials based on the response surface methodology," *Journal of Building Engineering* 38, article 102208. DOI: 10.1016/j.jobe.2021.102208

Yu, Y., Guo, Y., Jiang, T., Li, J., Jiang, K., and Zhang, H. (2017). "Study on the ingredient proportions and after-treatment of laser sintering walnut shell composites," *Materials* 10(12), article 1381. DOI: 10.3390/ma10121381

Zhang, H., Liu, D, Guo, Y., and Li, J. (2021). "Forming properties of boxwood/ thermoplastic polyurethane fabricated by selective laser sintering," *Chemistry and Industry of Forest Products* (02), 17-23.

Article submitted: November 10, 2024; Peer review completed: April 2, 2025; Revisions accepted: April 7, 2025; Published: May 9, 2025.
DOI: 10.15376/biores.20.3.5348-5360